ACS APPLIED MATERIALS & INTERFACES

Research Article

www.acsami.org

Creation of Superhydrophobic Stainless Steel Surfaces by Acid Treatments and Hydrophobic Film Deposition

Lester Li,[†,‡] Victor Breedveld,[†] and Dennis W. Hess*[,†]

[†]School of Chemical and Biomolecular Engineering, Georgia Institute of Technology, 311 Ferst Drive, Atlanta Georgia 30332, United States

[‡]Institute of Paper Science and Technology, Georgia Institute of Technology, 500 10th Street Northwest, Atlanta, Georgia 30318, United States

ABSTRACT: In this work, we present a method to render stainless steel surfaces superhydrophobic while maintaining their corrosion resistance. Creation of surface roughness on 304 and 316 grade stainless steels was performed using a hydrofluoric acid bath. New insight into the etch process is developed through a detailed analysis of the chemical and physical changes that occur on the stainless steel surfaces. As a result of intergranular corrosion, along with metallic oxide and fluoride redeposition, surface roughness was generated on the nano- and microscales. Differences in alloy composition between 304 and 316 grades of stainless steel led to variations in etch rate and different levels of surface roughness for similar etch times. After fluorocarbon film deposition to lower the surface energy, etched samples of 304 and 316 stainless steel displayed maximum static water contact angles of 159.9 and 146.6°, respectively. However, etching in HF also caused both grades of stainless steel to be susceptible to corrosion. By passivating the HF-etched samples in a nitric acid bath, the corrosion resistant properties of stainless steels were recovered. When a three step process was used, consisting of etching, passivation and fluorocarbon deposition, 304 and 316 stainless steel samples exhibited maximum contact angles of 157.3 and 134.9°, respectively, while maintaining corrosion resistance.

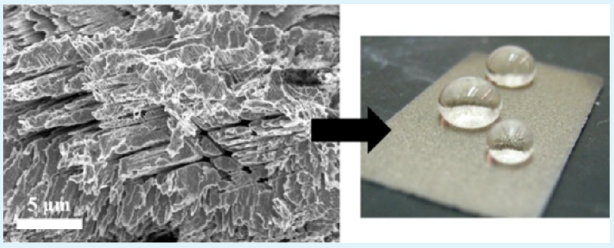

KEYWORDS: *superhydrophobic, stainless steel, 304, 316, hydrofluoric acid, selective etch*

1. INTRODUCTION

Over the past decade, superhydrophobic (SH) surfaces, which are defined as having a static contact angle (CA) greater than 150°, have been extensively studied[1−4] and fabricated on a variety of substrates including fabrics,[5] polymers,[4,6,7] glass[8,9] and metals.[10] Superhydrophobic metals are of great interest for industrial applications because of their special wetting properties, such as self-cleaning,[11,12] drag reduction[13−15] and corrosion resistance;[16,17] these features generally require that the high static contact angle is combined with low droplet adhesion (as defined by a low contact angle hysteresis).[10,12,18] Copper, aluminum, titanium and numerous metallic alloys have been surface modified to attain SH properties.[10,19] To ensure that these metals display SH properties, surface roughness at the proper length scale and a low surface energy are required. Techniques used for the creation of surface roughness on metals include electroless deposition,[20] sol−gel methods,[21] and anodization.[22] Fluorinated molecules are commonly used to achieve the necessary low surface energy.

Since the discovery in 1905 that iron alloyed with chromium is resistant to acid attack, stainless steel (SS) has been employed for applications in a wide range of fields, including petrochemical, construction, maritime and aviation industries.[23,24] Its broad use is the result of a unique and useful combination of high corrosion resistance and excellent mechanical strength. Industries where metal−fluid contact is common would benefit greatly from SH stainless steel surfaces. For example the food industry frequently uses SS vessels to store and mix fluids. The antifouling and corrosion resistant properties afforded by SH surfaces will reduce the need for cleaning, and thus reduce equipment/process down-time. The low hysteresis properties attained in our studies will also allow complete dewetting of tanks and pipes, thereby reducing loss of product due to residual surface wetting and adhesion. Furthermore, low hysteresis SH surfaces have been demonstrated to reduce fluid drag in pipe flow.[13] Despite this wide range of potential applications, fabrication of SH stainless steel has been relatively unstudied when compared to the other metals listed above. The majority of published work either uses ablation with a femtosecond laser to create the appropriate surface roughness,[25−27] which is not an easily scalable process, or coats the SS with another material to add roughness,[21,28−30] a process that often lacks mechanical durability.

To find a more scalable process to create robust SS surfaces with SH properties, we exploit the fact that surfaces of solid materials are often heterogeneous with regards to chemical composition and/or structure. If the heterogeneity occurs at suitable length scales, and if a selective etching method can be

Received: May 21, 2012
Accepted: August 20, 2012
Published: August 22, 2012

   dx.doi.org/10.1021/am301666c | ACS Appl. Mater. Interfaces 2012, 4, 4549−4556

found, it is then possible to create surface roughness. Using this paradigm, our group has produced low hysteresis SH paper substrates: selective etching of the amorphous phase of cellulose in an oxygen plasma, while leaving the crystalline phase, creates surface roughness at the required length scale.[31] The same approach has been applied to other polymer surfaces.[32] The key advantage of generating roughness directly on a material, as opposed to adding it through deposition of particles or residues, is the inherent mechanical stability of the structures that are formed via etching. Other researchers have used selective etching with an etchant mixture of ferric trichloride, hydrochloric acid and phosphoric acid to attack the less stable crystalline dislocation defects that exist in 304 SS; subsequent coating of the surface with a fluorosilane led to SH properties.[33] Although their work demonstrated that etching with ferric chloride can generate SH surfaces on 304 SS, no characterization of the chemical and physical effects of the etch process on SH properties was presented. Furthermore, the dependence of surface properties on etch parameters was not reported, nor were other SS alloys studied. To tailor and control SS wetting properties for specific applications and to ensure that the surface inhibits corrosion, it is necessary to relate the etch process to SS surface structure, chemical composition, and wetting characteristics in more detail.

Stainless steel is a broad term used to describe iron-based metals that contain greater than 12% chromium and have resistance to corrosive environments. SS alloyed compositions vary greatly based upon the desired application, with different alloy mixtures imparting varying corrosion resistance, hardness and mechanical strength. Iron−chromium-nickel alloys are known as the 300 series of SS, and are the most commonly used. 304 SS is composed of 18 wt % chromium and 8 wt % nickel, with iron making up the majority of the remaining composition. 316 SS has a similar composition, with the primary difference being the addition of 2−3 wt % molybdenum.

In this manuscript, we present a simple method to fabricate SH stainless steel surfaces by invoking hydrofluoric (HF) acid etching. Instead of the deposition of a secondary material to establish roughness, chemical etching is used to create surface roughness that maintains the mechanical and corrosive properties of the SS. Although HF acid is known to attack stainless steels, characterization of the surfaces formed by the concentrated acid etch has not been reported. The ability of this method to create roughness on two commonly used SS alloys, 304 and 316, is demonstrated. Alloy composition differences between these two grades of SS cause varied etch rates and surface structures, leading to different wetting properties. Our current study focuses both on the SH properties that our process generates and on the chemical changes needed to initially create the appropriate roughness. The etching process selectively attacks grain boundaries through intergranular corrosion and thus leads to the formation of micrometer and submicrometer scale roughness. On 316 SS, we demonstrate the enrichment of molybdenum on the surface grains after HF etching. By passivating the etched samples in nitric acid, the advantageous corrosion resistant properties of SS are re-established. Despite the fact that the effect of chemical passivation on stainless steels has been studied previously, the combination of passivation with a HF acid etch to form the appropriate surface roughness to create SH stainless steels has not been explored to date. Specifically, the passivation step causes separation of the martensitic-austenitic phase boundaries on 304 SS samples, creating a multiscale roughness that greatly differs from the roughness created in the etch step. Subsequent plasma deposition of a covalently bonded fluoropolymer layer then yields high water CAs and low hysteresis on both SS grades.

2. EXPERIMENTAL PROCEDURES

Etching and Passivation. 304 SS samples were obtained from Trinity Brand Industries and 316 SS samples were obtained from Maudlin Products, both in the form of 8 × 12 × 0.02 in. shim sheets. Etching was performed at 25 and 50 °C using a 48−51% hydrofluoric acid solution (ARISTAR, ACS grade). Unpassivated samples were rinsed with deionized (DI) water immediately after removal from the HF acid etch bath. The passivated samples, immediately after removal from the HF acid etch bath, were placed in a DI water bath, rinsed with DI water, and placed in a 50% nitric acid (ARISTAR, ACS grade, 68−70%) bath at 50 °C for 30 min, following the procedure described by ASTM standard A380−06. After completion of passivation, samples were again rinsed with DI water.

Hydrophobic Film Deposition. After the final DI water rinse, both unpassivated and passivated samples were placed in a parallel plate RF (13.56 MHz) plasma reactor, where deposition of fluoropolymer was carried out at 110 °C and 120 W using a mixture of pentafluoroethane precursor (Praxair) at 20 SCCM and argon at 75 SCCM. The thickness of the fluoropolymer layer is ∼100 nm, which yields complete coverage of the surface. Detailed reactor configuration and experimental deposition parameters have been described previously.[31] The result of the deposition is a highly cross-linked fluoropolymer layer that is covalently bonded to the SS surface.

Contact Angle Measurements. Static and dynamic contact angles were measured on a Rame-Hart contact angle goniometer (Model 100, Netcong, NJ). Static contact angles were measured by placing 4 μL droplets of DI water onto the substrate. Advancing CA measurements were performed starting with a 4 μL droplet and increasing the droplet volume by 1 μL increments until the droplet volume was 10 μL. Receding CA measurements were then performed by decreasing the volume of the 10 μL droplet in 0.5 μL steps until reaching the initial volume of 4 μL.

Profilometer Measurements. Average roughness (R_a) was measured using a Wyko NT2000 Optical Profilometer. Measurements were analyzed using the Vison32 (Veeco Instruments Inc.) analysis software. The average roughness was calculated per the ANSI B46.1 standard.

Surface Analyses. X-ray photoelectron spectroscopy (XPS) analyses were conducted using a Thermo Electron Corporation K-Alpha XPS system employing a microfocused monochromatic Al Kα X-ray source, with a 400 μm spot size. Samples were prepared for XPS by heating in a vacuum oven at 150 °C overnight. Scanning electron microscopy (SEM) images were taken with a Zeiss Ultra60 FE-SEM at an electron energy of 10.0 keV. Energy-dispersive X-ray spectroscopy (EDX) was performed using an integrated INCA EDX detector (Oxford Instruments) at an electron energy of 15 keV.

3. RESULTS AND DISCUSSION

For the sake of clarity, samples treated with the HF etch, passivation, and fluoropolymer coating steps will be denoted by (E), (P), and (F), respectively. For example, a sample designated 304(EF) SS has been etched and coated with a fluoropolymer, but not received the passivation treatment.

3.1. Hydrofluoric Acid Etching. To fully characterize and understand the SH surfaces generated by our process,we must first examine the means by which surface roughness is created. The mechanisms of the etch and passivation steps define the size, distribution, roughness and stability of the structures. Therefore, prior to presenting CA measurement data, we discuss in detail the chemical and physical effects of the etching and passivation steps on the stainless steels. Hydrofluoric (HF)

acid is commonly used for the pickling of stainless steel; in this process, a mixture of nitric and HF acids is used to remove surface contamination. The cleaning process occurs through competing HF etching and nitric acid passivation reactions, which continue until the surface has been cleaned. In contrast, when SS samples are etched in a corrosive environment without an oxidizer, as in our HF acid etch, the chemical reaction continues without hindrance, eventually leading to a roughened surface. During the HF acid etch process, SS samples change from their well-known, shiny silver appearance to black due to the added surface roughness and changes in chemical surface composition. Simultaneously, the HF acid solution turns green, a color that is characteristic of iron and chromium fluorides. XPS analyses of the surface composition of 304(E) and 316(E) SS after varied etch times are presented in Figures 1 and 2. In

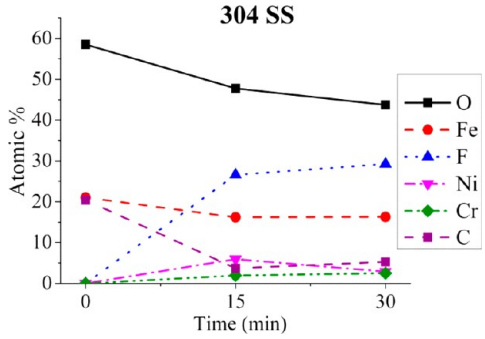

Figure 1. XPS analysis of 304(E) SS after 0, 15, and 30 min of etching at 50 °C.

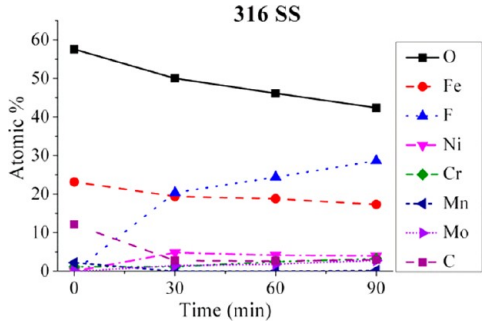

Figure 2. XPS analysis of 316(E) SS after 0, 30, 60, and 90 min of etching at 50 °C.

both cases, decreases in oxygen and iron atomic percentages are observed with longer etch times, while the fluorine concentration increases, indicating the formation of metallic fluorides. The deviation observed in Ni concentration in both samples is within the measurement variability of ±1.5 at % for all sample sets.

Figure 3 presents XPS spectral scans for chromium and iron on 304(E) SS after various HF etch times at 50 °C. Before etching, elemental chromium (574.0 eV) and iron (707.2 eV) are present on the surface along with Cr_2O_3 (577.1 eV) and Fe_2O_3 (710.9 eV). With an increase in etch time, the elemental metal peaks disappear, which corresponds to their conversion to oxides and fluorides. Close inspection of the XPS spectra reveals the development of shoulders at higher binding energies with increased etch time for both Cr and Fe. Deconvolution of the spectra indicates that these shoulders correspond to the formation of CrF_3 and FeF_3 at 579.1 and 714.2 eV, respectively.

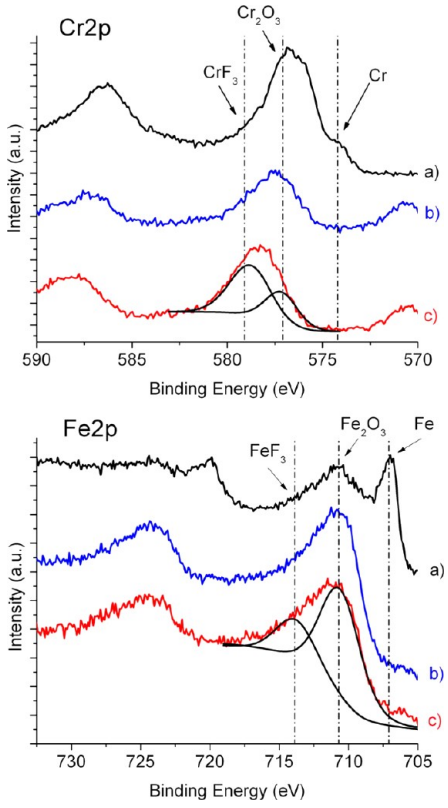

Figure 3. XPS scans of Cr2p and Fe2p on 304(E) SS: (a) before etching, and after (b) 15 and (c) 30 min of etching. Peaks in the 585–590 and 720–725 eV range correspond to the $2p_{1/2}$ peaks of Cr and Fe, respectively.

The Gaussian–Lorentzian deconvolution curves for the samples etched for 30 min are shown in Figure 3. Previous studies that described the etching of 304 SS in 40% HF at 40 °C have reported similar XPS results.[34]

Through the redeposition of metallic fluorides and oxides, roughness is created at micrometer and submicrometer lengths. Figure 4a presents an image of petal-like structures on 304(E) SS etched for 5 min in HF acid at 50 °C; these structures, which are reminiscent of fractal geometries, have been shown to be characteristic of iron oxide.[35] Similar structures are also, to a lesser extent, present on etched 316(E) SS samples, with formation mainly occurring between grains. The effects of fractal structures on the SH surface properties have been previously modeled and observed.[36,37] Although further studies are needed to characterize the fractal nature of our samples and determine the specific role that such structures play in the superhydrophobicity, these studies are beyond the scope of the current investigation. Iron fluoride, chromium fluoride and chromium oxide have been reported to have granular crystalline structures, similar to those shown in Figure 4b.[38,39] The precipitation of both FeF_3 and CrF_3 from acidic baths has been demonstrated previously for the case of SS pickling. Specifically, if a pickling bath is not continuously replenished, precipitation of metal fluorides can occur,[40] with FeF_3 being of greater concern because of the high concentration of iron in SS. No intentional solution agitation was used during our etch process, which allowed concentration gradients to form near the surface of the stainless steel during the reaction with HF. When the solution becomes locally supersaturated, fluorides and oxides can precipitate to form the observed surface roughness.

dx.doi.org/10.1021/am301666c | ACS Appl. Mater. Interfaces 2012, 4, 4549–4556

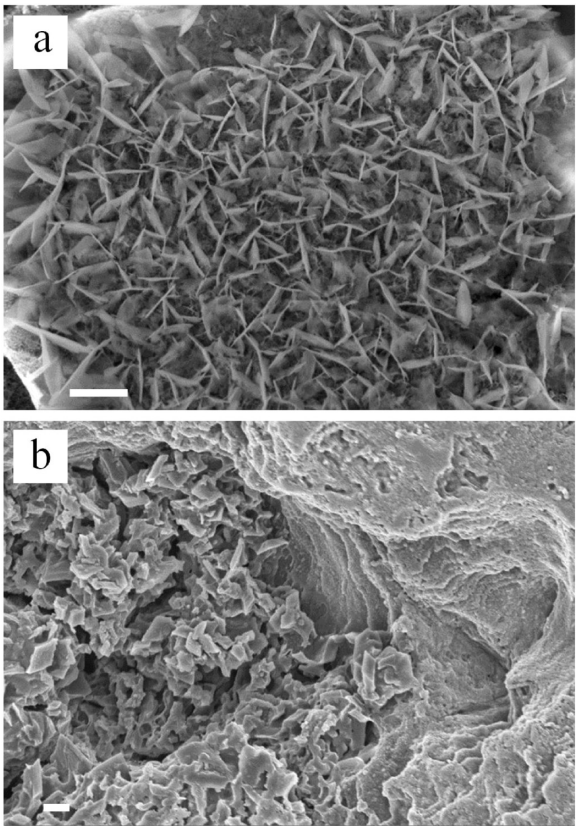

Figure 4. 304(E) SS etched for 5 min at 50 °C with: (a) petal-like structures that are indicative of Fe_2O_3, (b) granular structures of FeF_3 and CrF_3. White scale bars correspond to 1 μm.

Although the aforementioned structures form rapidly on 304 SS, their evolution occurs at a much slower rate on 316 SS. The predominant difference between the two grades of SS is the presence of molybdenum in 316 SS, which without passivation is not present on the topmost surface.[41] Figure 2 shows an increase in molybdenum concentration from 0% before etching, to maximum of 3.0% after 90 min of etching. Energy-dispersive X-ray (EDX) analysis on the same sample (data not shown) demonstrates further enrichment throughout the underlying layer with a molybdenum concentration of 6.7%; it should be noted that XPS analysis only probes the top 10 nm surface layer, whereas EDX samples up to 5 μm in depth, thus allowing EDX to give a more complete analysis of the composition of the structures formed. The surface enrichment of molybdenum is a consequence of its resistance to HF acid etching.[42,43] Figure 5 shows spatial EDX mapping of the surface of a 90 min HF acid etched 316(E) SS sample. The mapping shows increased molybdenum on the remaining grains, whereas the grain boundary regions show increased chromium and iron concentrations.

3.2. Passivation. In an oxygenated atmosphere, SS spontaneously forms a passivating chromium oxide layer, imparting corrosion resistance to SS. During the HF etch, the passivation layer is removed, exposing an iron rich surface that cannot re-establish passivation at ambient conditions. Figures 1 and 2 show a minimal chromium surface concentration on both SS types after etching in HF, while the percentage in the bulk alloy is 18 wt %. The lack of chromium at the surface inhibits formation of a passive oxide layer, resulting in a weakly adherent iron oxide and fluoride layer. When exposed to

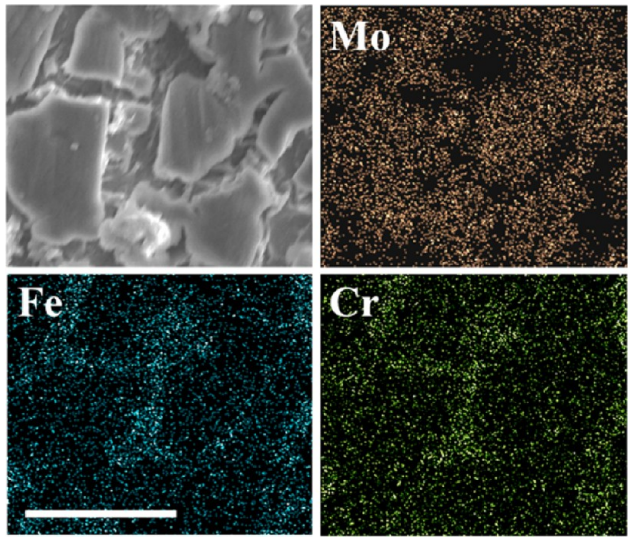

Figure 5. EDX mapping of molybdenum, iron and chromium on 316(E) SS etched for 90 min. The images show enrichment of molybdenum on the remaining grains, whereas iron and chromium are depleted in those areas. White scale bar represents 20 μm.

ambient conditions, unpassivated and uncoated SS samples therefore form an orange-colored iron oxide layer within one day of the HF etch. In addition, after the etch step, SS surfaces are covered by metal oxide and metal fluoride particles that display weak adhesion to the surface. Even a high velocity water jet from a standard wash bottle is sufficient to remove the precipitated structures from the surface. Both of these characteristics, lack of corrosion resistance and poor mechanical stability, are undesired outcomes of the HF etching process. By exposing the etched samples to nitric acid, the corrosion resistant properties of SS are restored.

The nitric acid bath treatment restores the SS passivation layer through the consumption of exogenous iron, as well as iron and chromium fluorides on the surface, thus allowing chromium to form a passive oxide layer on the surface. Figures 6 and 7 show the effect of passivation on 304 and 316 SS etched at 50 °C, respectively, with a noticeable difference in surface roughness before and after passivation. Figure 6a–e show SEM images of 304(E) and (EP) SS etched in HF acid at 50 °C, with and without passivation. Figure 6a shows an unetched 304 sample, whereas samples 304(E) SS in Figures 6b and 6c were etched in HF for 15 and 30 min, respectively, and panels d and e in Figure 6 display samples 304 (EP) SS that were etched for the same times and subsequently passivated in nitric acid. For both etch times, the passivation step effectively removes micrometer scale granular and crystalline roughness, exposing a flakelike structure.

Figure 7a shows SEM images of an untreated sample of 316 SS. Images b and d and images c and e in Figure 7 show the surface before and after passivation after 60 and 90 min of etching, respectively. In both sets of images, it is evident that the passivation step removes much of the microscale roughness, exposing a large granular structure that greatly differs from the structures seen on 304(EP) SS (Figure 6). Again, intergranular corrosion appears to be the primary method of chemical attack, as is evident in images b and c in Figure 7.

Samples of 316 SS experience a near complete removal of the surface structures. Nitric acid is known to readily dissolve molybdenum under the experimental conditions used here.[44]

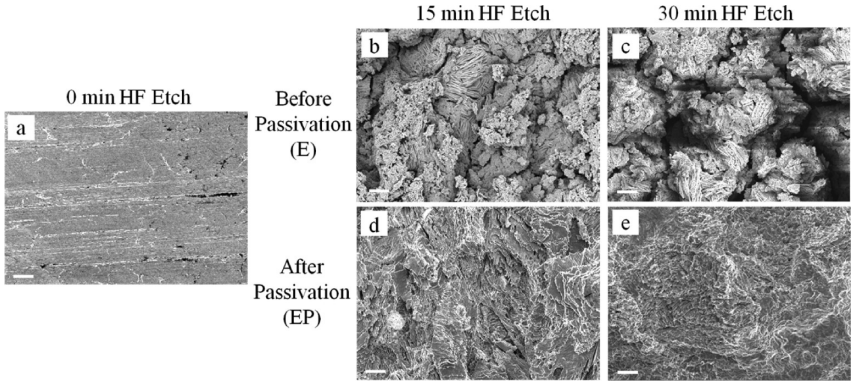

Figure 6. SEM images of unpassivated (E) and passivated (EP) HF acid etched (50 °C) 304 SS for 0, 15, and 30 min etch times. White bars correspond to 10 μm.

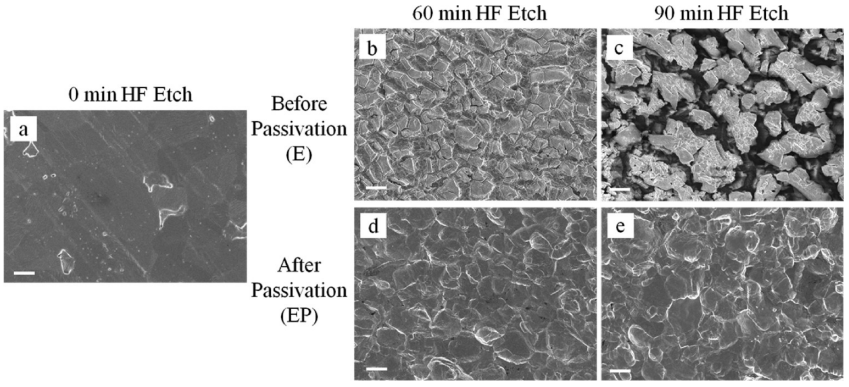

Figure 7. SEM images of unpassivated (E) and passivated (EP) HF acid etched (50 °C) 316 SS for 0, 30, 60, and 90 min etch times. White bars correspond to 10 μm.

The surface structures that remain after passivation of 316 SS are the grains of the underlying SS. A higher-magnification image of the surface of 316(EP) SS is shown in Figure 8a, with individual grains clearly visible. In contrast, the surface of 304(EP) SS remains roughened even after passivation. Although the surface structure has been drastically changed by the passivation, it maintains its micrometer and submicrometer scale roughness, as shown in Figure 8b. XPS analysis after passivation (not shown) demonstrates the disappearance of the fluoride peaks for both iron and chromium, indicating that surface passivation has occurred on both SS types. Removal of the weakly adherent metallic fluorides in the passivation step reexposes the native SS, thus recovering the inherent mechanical strength of the underlying SS in the surface structures. More detailed physical durability testing of the surfaces is planned for future studies. The structures observed on 304(EP) SS after passivation have been reported before, albeit without a conclusive explanation of the mechanism.[45] It is our interpretation that the flake-like structure of passivated 304 SS is attributed to the cold rolling manufacturing process of the 304 SS shim sheets, which creates microstructures of deformation-induced martensite inclusions within austenitic grains.[46] The weakening of the microstructure boundaries during the HF acid etch allows nitric acid to selectively remove the martensitic phase. Well-defined etch lines along these grain boundaries are visible in Figure 8b. It has also been demonstrated that under the same cold rolling conditions, 316 SS forms significantly less martensite, explaining structural differences after passivation.[46]

3.3. Reestablishment of Chemical Passivity. Passivated samples were further tested for passivity using a standardized copper sulfate test (ASTM A380−06), during which a mixture of DI water, copper sulfate and sulfuric acid is placed on the surface of the metal. The existence of unalloyed iron on the surface would lead to the formation of metallic copper on the surface, which can readily be detected visually. Since this test was negative on our etched and passivated (EP) SS samples, it can be concluded that the passivation step successfully removes exogenous iron from the surface. Although extensive electrochemical corrosion studies are outside the scope of this study, preliminary experiments were conducted to demonstrate the establishment of a corrosion resistant, passivated surface. Similar thicknesses of plasma-deposited fluoropolymer films to those used in our studies have been shown to increase the corrosion resistance of carbon steel substrates.[47] In this study, samples of 304 and 316 (EP) and (EPF) stainless steels were placed in a 5 wt % sodium chloride solution at 50 °C. We observed that both (EP) and (EPF) samples of stainless steels exhibited corrosion resistance analogous to that of untreated samples, with all samples resisting surface discoloration for 15 days. In strong contrast, samples of 304 and 316(EF) stainless steels showed poor corrosion resistance. The samples discolored rapidly and spalled off the weakly adherent particle layer in less than 12 h, thus exposing the underlying SS to continued corrosion. These preliminary tests highlight the importance of the passivation step in recovering the desirable corrosion resistance of stainless steel.

3.4. Contact Angle Measurements on 304 Stainless Steel. The previous sections focused on chemical modifications

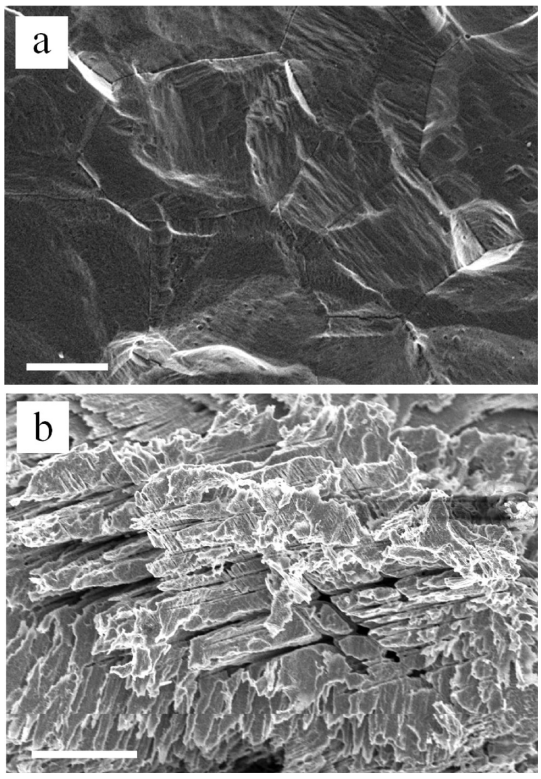

Figure 8. High-magnification images of: (a) 90 min etched 316(EP) SS, and (b) 30 min etched 304(EP) SS at 50 °C. White bars correspond to 5 μm.

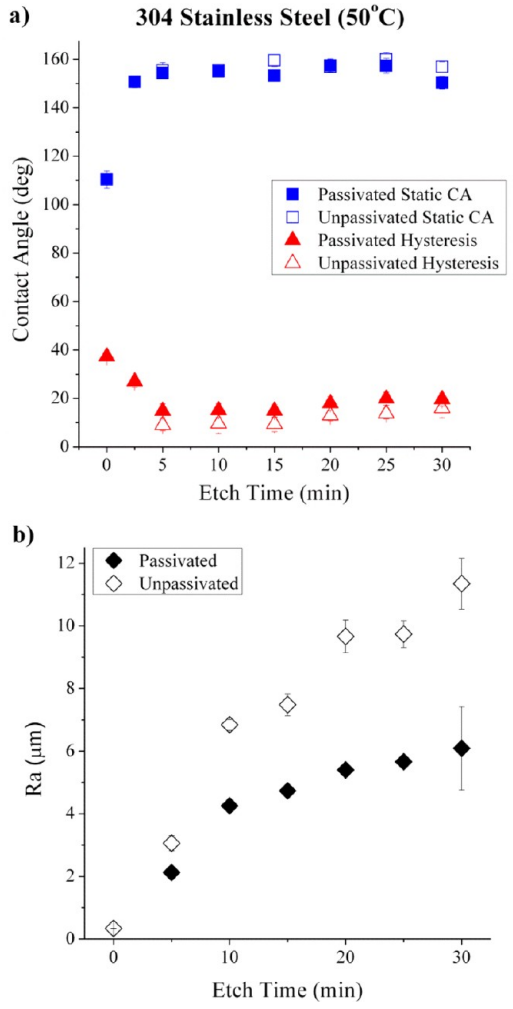

Figure 9. (a) Static contact angles and hysteresis, and (b) mean roughness measurements of passivated (EPF) and unpassivated (EF) 304 SS as function of duration of HF acid etch (50 °C).

due to the etch and passivation steps; that is, samples were analyzed prior to fluoropolymer deposition (with the corrosion tests as the only exception). In the following (sections 3.4 and 3.5), we shift focus to the effects of surface structure on CA; as a consequence, samples with fluoropolymer coating are mainly discussed, except for a few relevant control samples.

Before processing, as received samples of 304 SS display a CA of 87.4° ± 3.0. After passivation, without HF acid etch or fluoropolymer deposition, 304(P) SS shows a reduced CA of 75.2° ± 2.4. This decrease is likely the result of removal of surface contamination imparted by the SS cold rolling process during passivation.

Figure 9 shows the static CAs, hysteresis, and mean roughness of 304 (EF) and (EPF) SS etched with HF acid at 50 °C as a function of etch time. Without the fluoropolymer coating, both (E) and (EP) samples are hydrophilic (CA < 20°) at all etch times because of changes in chemical and physical surface properties. Fluoropolymer thickness is not expected to play a significant role in the observed roughness due to the length scale of the deposition layer (~100 nm) compared to the roughness measured (micrometer scale). The etch reaction proceeds rapidly upon immersion of the sample in the HF acid bath, with vigorous bubbling and immediate surface roughening; 5 min of etching increased the CA from 110.4° ± 3.7 to 155.3 ° ± 3.3 after fluoropolymer deposition.

Figure 9b indicates that as etch time is increased, the mean roughness also increases, with unpassivated samples having a greater roughness at all etch times. As previously discussed, the passivation step removes the roughness created by the redeposition of metallic fluorides, exposing the martensitic-austenitic phase boundaries shown in Figure 6. When comparing panels a and b in Figure 9, it is clear that the prolonged etch and increased mean roughness have little effect on the static CA. After the first 5 min of etching, neither extended etching nor chemical passivation has an appreciable effect on the static CA. Unlike the static CA, the hysteresis increases slightly after passivation. The hysteresis reaches a minimum after 5 min of etching both before and after passivation, and then slowly increases with increasing etch time.

Fabrication of SH 304 SS through HF acid etch was also performed at room temperature (25 °C). Figure 10 presents CA data of (EF) and (EPF) samples and the mean surface roughness for different etch times.

When compared to 304 SS samples etched at 50 °C, the (EF) samples etched at 25 °C exhibit a slower increase in CA and slower decrease in hysteresis. (EPF) samples, however, still rapidly attain high CAs and low hysteresis. Although the R_a values after 30 min of etch and passivation vary greatly at the two different temperatures (6.09 μm ± 1.33 at 50 °C and 3.78 μm ± 0.35 at 25 °C), the static and dynamic CAs are similar. It appears that the passivated samples are less affected by etch temperature. This is believed to be due to the fact that the acid etch weakens the martensitic-austenitic phase boundaries and thereby allows the nitric acid passivation to separate the phases and create the specific surface structures required for high CAs. As shown in Figure 6, the passivation step creates a flakelike

dx.doi.org/10.1021/am301666c | ACS Appl. Mater. Interfaces 2012, 4, 4549−4556

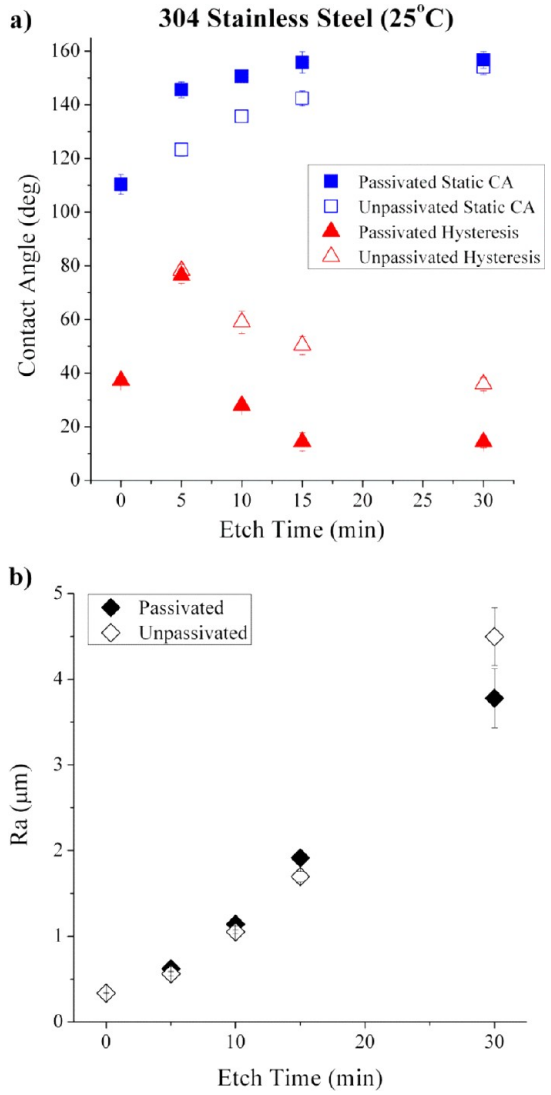

Figure 10. (a) Static contact angles and hysteresis, and (b) mean roughness measurements of passivated (EF) and unpassivated (EPF) 304 SS as function of duration of HF acid etch (25 °C).

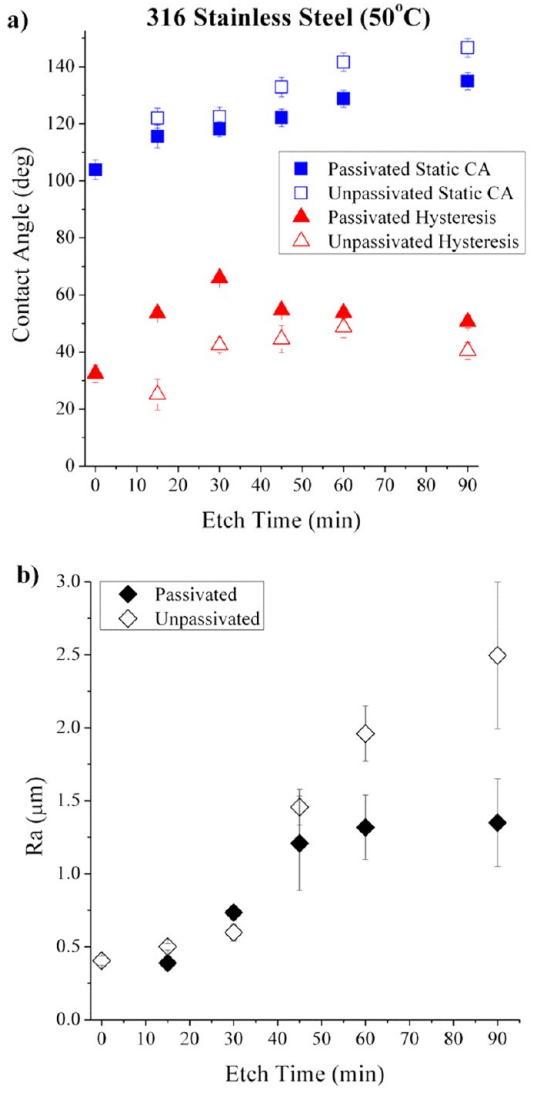

Figure 11. (a) Static contact angles and hysteresis, and (b) mean roughness measurements of passivated (EF) and unpassivated (EPF) 316 SS as function of duration of HF acid etch (50 °C).

structure from the unpassivated granular structure, thus allowing high CAs even at relatively low mean roughness values.

3.4. Contact Angle Measurements on 316 Stainless Steel. Figure 11a shows static CAs and hysteresis values of 316(EP) and (EPF) SS, while Figure 11b shows the mean roughness. Apparently due to manufacturing contamination issues, the CA of as received 316 SS was highly variable; after passivation and removal of surface contamination, the CA was 60.2° ± 2.8. Fluoropolymer deposition increases the CA of 316(F) SS sample to 103.9° ± 3.4. Similar to 304 SS, without fluoropolymer deposition, the acid etch and passivation steps render the 316 grade SS samples hydrophilic (CA < 20°) for all etch times. The reaction of 316 SS in HF acid occurs at a visibly slower rate, requiring longer times before signs of etching are evident, for instance through the observation of bubble formation. Comparison of R_a values for 304 and 316 SS (Figures 9b and 11b) indicates that surface roughness generation on 316 SS occurs at a markedly slower rate than that observed for 304 SS. After 90 min of HF acid etch, a sample of 316(EF) SS has R_a = 2.5 μm ± 0.5, whereas after only 5 min of etching, a sample of 304(EF) SS has already exceeded that value (R_a = 3.06 μm ± 0.25). The reduced rate of surface roughness formation on 316 SS, along with the granular structure of the roughness, explains the lowered CAs when compared to 304 SS for similar etch times. The increased hysteresis observed in 316 SS samples is most likely due to wetting in the Wenzel state, while 304 SS samples have the characteristics of a Cassie–Baxter state.[12] For both unpassivated and passivated samples it is obvious that as etch time is increases, the static CA increases as well, with the maximum average CA reaching 146.6° ± 3.2 after 90 min of etching for the unpassivated sample (after fluoropolymer deposition). Unlike 304 SS, passivation of 316 SS notably decreases the static CA by an average of 9.1°.

4. CONCLUSIONS

By etching 304 and 316 SS samples in HF acid, followed by passivation in nitric acid and fluoropolymer deposition, we have demonstrated the ability to create superhydrophobic SS surfaces that maintain the corrosive properties of untreated stainless steels, while changing the wetting properties

dx.doi.org/10.1021/am301666c | ACS Appl. Mater. Interfaces 2012, 4, 4549–4556

significantly. Both types of SS are initially etched through intergranular corrosion. As etch times increase, 304 SS forms micrometer and submicrometer scale surface roughness due to the formation of iron and chromium oxides and fluorides, with a sample of 304(EF) SS achieving a CA of 159.9° ± 2.8 and a hysteresis of 13.7° ± 2.2 after 25 min of etching at 50 °C. The ability to etch 304 SS at 25 °C was also demonstrated, attaining a CA of 156.7° ± 3.0 and a hysteresis of 14.4° ± 2.2 with the (EF) treatments. Due to the molybdenum content in 316 SS, the etch rate is significantly reduced, resulting in decreased roughness. For a sample of 316(EF), the reduced etch rate leads to a maximum CA of 146.6° ± 3.2 with a hysteresis of 40.4° ± 2.9 after 90 min of etching. However, after HF acid etching, both types of SS are no longer corrosion resistant, because the passivation layer has been removed by the etch process.

Chemical passivation in nitric acid was employed to restore the beneficial corrosion resistant properties that are characteristic of SS. Through the removal of iron and metallic fluorides, the passive chromium oxide layer is restored, while the remaining surface roughness leads to sustained high CAs and low hysteresis. A static CA of 157.3° ± 2.8 was found on 304(EPF) SS that was etched for 25 min at 50 °C. The three-step process described provides a simple method of fabricating SH stainless steel surfaces, while maintaining corrosion resistance.

AUTHOR INFORMATION

Corresponding Author

*E-mail: dennis.hess@chbe.gatech.edu.

Notes

The authors declare no competing financial interest.

ACKNOWLEDGMENTS

The authors thank Dr. Ashwini Sinha (Praxair) for generously donating the pentafluoroethane (PFE) gas and Dr. Preet Singh (Georgia Tech) for helpful data interpretation and discussions. The authors are also grateful to the Institute for Paper Science and Technology (IPST) at Georgia Tech for fellowship support for L.L.

REFERENCES

(1) Sun, T. L.; Feng, L.; Gao, X. F.; Jiang, L. *Acc. Chem. Res.* **2005**, *38*, 644.

(2) Li, X. M.; Reinhoudt, D.; Crego-Calama, M. *Chem. Soc. Rev.* **2007**, *36*, 1350.

(3) Roach, P.; Shirtcliffe, N. J.; Newton, M. I. *Soft Matter* **2008**, *4*, 224.

(4) Ahuja, A.; Taylor, J. A.; Lifton, V.; Sidorenko, A. A.; Salamon, T. R.; Lobaton, E. J.; Kolodner, P.; Krupenkin, T. N. *Langmuir* **2008**, *24*, 9.

(5) Ma, M. L.; Mao, Y.; Gupta, M.; Gleason, K. K.; Rutledge, G. C. *Macromolecules* **2005**, *38*, 9742.

(6) Bormashenko, E.; Stein, T.; Whyman, G.; Bormashenko, Y.; Pogreb, R. *Langmuir* **2006**, *22*, 9982.

(7) Shiu, J. Y.; Kuo, C. W.; Chen, P. L.; Mou, C. Y. *Chem. Mater.* **2004**, *16*, 561.

(8) Nakajima, A.; Hashimoto, K.; Watanabe, T.; Takai, K.; Yamauchi, G.; Fujishima, A. *Langmuir* **2000**, *16*, 7044.

(9) Nakajima, A.; Fujishima, A.; Hashimoto, K.; Watanabe, T. *Adv. Mater.* **1999**, *11*, 1365.

(10) Liu, K. S.; Jiang, L. *Nanoscale* **2011**, *3*, 825.

(11) Furstner, R.; Barthlott, W.; Neinhuis, C.; Walzel, P. *Langmuir* **2005**, *21*, 956.

(12) Lafuma, A.; Quere, D. *Nat. Mater.* **2003**, *2*, 457.

(13) Shirtcliffe, N. J.; McHale, G.; Newton, M. I.; Zhang, Y. *ACS Appl. Mater. Interfaces* **2009**, *1*, 1316.

(14) Ou, J.; Rothstein, J. P. *Phys. Fluids* **2005**, *17*, 103606.

(15) Choi, C. H.; Kim, C. J. *Phys. Rev. Lett.* **2006**, *96*, 066001.

(16) Liu, H. Q.; Szunerits, S.; Xu, W. G.; Boukherroub, R. *ACS Appl. Mater. Interfaces* **2009**, *1*, 1150.

(17) Liu, T.; Chen, S. G.; Cheng, S.; Tian, J. T.; Chang, X. T.; Yin, Y. S. *Electrochim. Acta* **2007**, *52*, 8003.

(18) Ma, M. L.; Hill, R. M. *Curr. Opin. Colloid Interface Sci.* **2006**, *11*, 193.

(19) Qian, B. T.; Shen, Z. Q. *Langmuir* **2005**, *21*, 9007.

(20) Wu, W. C.; Chen, M.; Liang, S.; Wang, X. L.; Chen, J. M.; Zhou, F. *J. Colloid Interface Sci.* **2008**, *326*, 478.

(21) Zhang, X. X.; Honkanen, M.; Jarn, M.; Peltonen, J.; Pore, V.; Levanen, E.; Mantyla, T. *Appl. Surf. Sci.* **2008**, *254*, 5129.

(22) Wu, W. C.; Wang, X. L.; Wang, D. A.; Chen, M.; Zhou, F.; Liu, W. M.; Xue, Q. J. *Chem. Commun.* **2009**, 1043.

(23) Cobb, H. M., *The History of Stainless Steel*; ASM International: Materials Park, OH, 2010.

(24) Khatak, H. S.; Baldev, R., *Corrosion of Austenitic Stainless Steel: Mechanism, Mitigation and Monitoring*; ASM International: Materials Park, OH, 2002.

(25) Wu, B.; Zhou, M.; Li, J.; Ye, X.; Li, G.; Cai, L. *Appl. Surf. Sci.* **2009**, *256*, 61.

(26) Kietzig, A.-M.; Hatzikiriakos, S. G.; Englezos, P. *Langmuir* **2009**, *25*, 4821.

(27) Groenendijk, M.; Meijer, J. *J. Laser Appl.* **2006**, *18*, 227.

(28) Chen, L. J.; Zhao, J. W. *J. Dispersion Sci. Technol.* **2010**, *31*, 1245.

(29) Feng, L.; Zhang, Z. Y.; Mai, Z. H.; Ma, Y. M.; Liu, B. Q.; Jiang, L.; Zhu, D. B. *Angew. Chem., Int. Ed.* **2004**, *43*, 2012.

(30) Chen, L. J.; Chen, M.; Hui, H. D.; Chen, J. M. *Appl. Surf. Sci.* **2008**, *255*, 3459.

(31) Balu, B.; Breedveld, V.; Hess, D. W. *Langmuir* **2008**, *24*, 4785.

(32) Youngblood, J. P.; McCarthy, T. J. *Macromolecules* **1999**, *32*, 6800.

(33) Yu, N. J.; Yu, Y. F.; Li, Y. F.; Song, S. P.; Huo, S. B.; Han, X. Y. *Surf. Rev. Lett.* **2010**, *17*, 375.

(34) Xu, H. L.; Li, Y.; Jiang, D. Q.; Yan, X. P. *Anal. Chem.* **2009**, *81*, 4971.

(35) Zhong, L. S.; Hu, J. S.; Liang, H. P.; Cao, A. M.; Song, W. G.; Wan, L. J. *Adv. Mater.* **2006**, *18*, 2426.

(36) Hazlett, R. D. *J. Colloid Interface Sci.* **1990**, *137*, 527.

(37) Shibuichi, S.; Onda, T.; Satoh, N.; Tsujii, K. *J. Phys. Chem.* **1996**, *100*, 19512.

(38) Forsberg, K. M.; Rasmuson, A. C. *J. Cryst. Growth* **2010**, *312*, 2351.

(39) Chen, L. F.; Song, Z.; Wang, X.; Prikhodko, S. V.; Hu, J. C.; Kodambaka, S.; Richards, R. *ACS Appl. Mater. Interfaces* **2009**, *1*, 1931.

(40) Galvez, J. L.; Dufour, J.; Negro, C.; Lopez-Mateos, F. *Chem. Eng. J.* **2008**, *136*, 116.

(41) Rao, T. V.; Vook, R. W.; Meyer, W.; Joshi, A. *J. Vac. Sci. Technol. A* **1986**, *4*, 1604.

(42) Craig, B. D.; Anderson, D. S., *Handbook of Corrosion Data*; ASM International: Materials Park, OH, 1995.

(43) Gupta, C. K., *Extractive Metallurgy of Molybdenum*; CRC Press: Boca Raton, FL, 1992.

(44) *DECHEMA Corrosion Handbook—Revised and Extended 2nd Edition*; Society for Chemical Engineering and Biotechnology (DECHEMA): Frankfurt, Germany, 2008.

(45) Mayuzumi, M.; Ohta, J.; Arai, T. *Corrosion* **1998**, *54*, 271.

(46) Hadji, M.; Badji, R. *J. Mater. Eng. Perform.* **2002**, *11*, 145.

(47) Delimi, A.; Galopin, E.; Coffinier, Y.; Pisarek, M.; Boukherroub, R.; Talhi, B.; Szunerits, S. *Surf. Coatings Technol.* **2011**, *205*, 4011.